Synthesis and microstructural characterization of nanostructured CuO particles

A.-G. PLAIASU[a*], A. DINU[b], D. NEGREA[a], V. RIZEA[a], M. M. DICU[a], D. BOJIN[c], M. ABRUDEANU[a], J. C. MONTY[d], M. ENACHESCU[c], E.S. BARCA[a], C. MUNTEANU[e]
[a]*University of Piteşti, 1 Targu din Vale Street, 110040, Pitesti, Romania*
[b]*ICN, The Institute for Nuclear Research, 1 Campului Street, 115400, Mioveni, Romania*
[c]*University "Politehnica" of Bucharest, Center of Surface Science and Nanotechnology, 313 Splaiul Independentei, 060042, Bucharest, Romania*
[d]*CNRS-PROMES, 7 Rue du Four Solaire Street, Odeillo, 66120, Font Romeu, France*
[e]*"Gheorghe Asachi" Technical University of Iasi, 41 Prof.dr.doc. D. Mangeron Street, 700050, Iaşi, Romania*

The oxides of copper are interesting materials due to their remarkable optical, electrical, thermal and magnetic properties. In nanostructured state can further enhance the performance of this important functional material and provide it with unique properties that do not exist in its bulk form. Elaboration with solar energy of CuO nanoparticles has not been reported yet in the literature. The paper aims and to present the most important results referring to the CuO nanoparticles obtained by SPVD (Solar Physical Vapor Deposition) process. The X-ray diffraction analysis (XRD) was chosen as the first method used to characterize these nano oxides powders. The average size of particles from diffraction domains of the analysed powders was compared to the average particle size determined by transmission electron microscopy. To complete the characterization X-ray Fluorescence analysis offers information about the chemical elemental composition of the nanopowders. The results prove that solar physical vapor deposition process to be an original process to prepare nanopowders.

(Received May 19, 2015; accepted June 24, 2015)

Keywords: Characterization, Nanoparticles, Oxide, Solar energy

1. Introduction

Researches on the elaboration and studies on properties of nanostructured materials are one of the most important topics at present. Grain boundaries make up a major portion of the material at nanoscales and strongly affect properties and processing. Due to the specific arrangement of atoms, the nanometric field is governed by numerous surface phenomena. From the general class of "nanomaterials" the nanopowders consist of grains (unorganized aggregates, nanocrystals or polycrystals) which have nanometric dimensions. The oxides based nanopowders can be manufactured by three generic routes: chemical, mechanical and gas phase synthesis [1-21]. The classical ceramic routes in producing nano-oxides through solid state reactions at high temperature have many disadvantages due to the large diffusion distances. New chemical methods such as hydrolysis, sol-gel process, hydrochemical synthesis or processes in gaseous phase have been developed to synthesize oxides nanopowders.

Nanostructured transition metal oxides are of great interest in the present research because of their interesting properties with a variety of applications. From this category CuO is an important p-type transition metal oxide with a narrow band gap (Eg¼1.2–1.9 eV) with wide application range in gas sensors, biosensors, solar cells, high Tc superconductors, medicine, lithium ion batteries, transistors, catalysts, etc. [1-14, 16-21]. The space group of its unit cell is C2/c, and its lattice parameters are a=4.6837, b=3.4226, c=5.1288, β=99.54^0 [1]. The copper atom is coordinated by 4 oxygen atoms in an approximately square planar configuration like in figure 1, obtained with CaRIne Crystallography software.

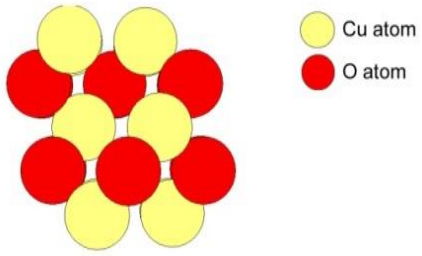

Fig. 1. Crystal structure of CuO

Because the chemical and physical properties of CuO are strictly dependent of its morphology, in latest years considerable efforts have been made to synthesize various types of CuO nanostructures including nanorods [3], nanoflowers [4], nanowires [11], nanospindles [12] and nanospheres [19, 21] have been synthesized by different methods. Moreover, a number of elements can be used as doping elements to enhance the physical and chemical properties of oxide. Many researches on the mixed oxide catalysts containing manganese oxides or copper oxides

were carried out but there are a few reports on Mn-doped bulk and/or nanostructured CuO.

Furthermore the elaboration of CuO nanoparticles pure and doped with Mn with solar energy has not been reported yet. In this context, the paper present and discuss the most important results discussing the CuO nano-powders doped with Mn, obtained by SPVD process.

2. Experimental

Solar physical vapor deposition (SPVD) is an original process to prepare nanostructured materials developed at Odeillo/Font Romeu, France, were built 12 solar furnaces which are organized by moveable plane mirrors ("heliostats") and a parabolic concentrator. At the focus of parabolic mirror, a 1 m^2 in surface, is placed a cooled holder or a reactor constituted by glass balloons. Inside, the raw material which is going to be melted and vaporized is placed on a cooled support at the focus. The vapor pressure all over the target strongly hangs on the type of material and on the atmosphere inside the solar reactor. Usually a visible smoke appears and condenses on a "cold finger" (cooled copper tubes with water) or on a ceramic filter [10]. The most recent reactor, the "heliotron", links the two processes mentioned before [14]. The quantity depends on the vapor pressure of the material (example: pure or doped zinc oxide it can reach several hundred milligrams per hour [10, 13, 14]. When the vapor pressure on the top of the melted material is low, the SPVD generated nanopowder quantity is less than 1 mg/hour even at flux higher than 1kW/m^2. It is one of the reasons why in that case, when large quantities are needed; a different process has been developed, associating melting in a solar furnace, quenching and ball milling [10, 13].

In our paper the raw material were obtained by mixing and pressing commercial CuO having purity of 99% and for doping it was used commercial MnO having a purity of 99% (purchased from Merck) and the view of solar reactor is presented in fig.2.

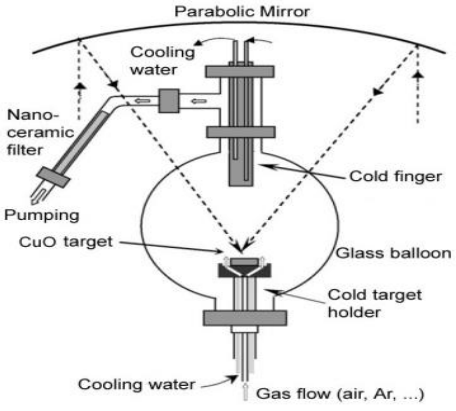

Fig. 2. Solar physical vapor deposition (SPVD) process in the solar reactor, view of the "heliotron" solar reactor

The density of solar flux and the air pressure in reactor needed for vapor-condensation are presented in the Table 1.

Table 1. Experimental parameters of elaboration

Air pressure reactor(hPa)	Density of solar flux (W/m^2)	Sample cod of nanopowders
50	967	VCCuO
	968	VC0.05MNCUO
	910	VC1MNCUO
	933	VC2.5MNCUO
	933	VC10MNCUO1

Fig. 3 shows the nanopowders collection by aspiration on a nanoporous ceramic filter and by condensation on a cold finger like. In the case of CuO all the nanophases are black color.

a)

b)

Fig. 3. Nanopowders are collected simultaneously on a ceramic filter (a) and on water cooled copper finger (b)

XRD analysis was performed at room temperature, using a PANalytical X' Pert Pro diffractometer operating at 40 kV and 20 mA (Cu Kαradiation, 0.15418nm). X-ray diffraction measurements of- symmetrical scans were made in the range 10° to 100°.

TEM analysis was performed using an EM-410 Philips microscope at room temperature. TEM images offer detailed information on the nanostructure and nanophases present in the nanopowders.

The X-ray Fluorescence Spectrometry (XRF) was chosen as fast and reliable method for chemical elemental analysis. It has a high accuracy especially for trace elements analysis having a detection range up to ppm level which makes it best as complementary analysis of XRD. The samples obtained by SPVD were analyzed with an Energy Dispersive X-ray Fluorescence (EDXRF) spectrometer in the following configuration: 30 W-Molybdenum X-ray tube which generates a measurement spot with 2 mm diameter and a Si Drift Detector (SDD) with 160 eV resolution (relative to the Mn-Kα line and an input pulse density of 1000 cps). For each sample a point scan was made. Two spectra have been acquired for each scan. For the first one it was used a voltage of 44.70 kV and a current of 0.30 mA, direct excitation, a 1.00 mm collimator and maximum measuring time of 180 s on 2048 channels. For the second spectra it was used a voltage of 18.87 kV and a current of 0.30 mA, direct

excitation, a 2 mm collimator and maximum measuring time of 300 s on 1024 channels.

3. Results and discussion

3.1. X-rays diffraction

The peaks obtained by XRD are characterized by diffraction angles θ_{hkl} and I_{hkl} intensities depending on the lattice cell and on the wavelength radiation, λ. The position of the diffraction peaks provides the distances d_{hkl} between crystallographic planes, the structure and the lattice parameters. The (hkl) Miller indexes correspond to the diffracting crystallographic planes characterized by the same interplanar distance d_{hkl} [10]. These three parameters are linked through the Bragg relation:

$$2d_{hkl} \sin \theta_{hkl} = n\lambda \quad (1)$$

The Fig. 4a presents the XRD patterns of the pure CuO and Mn doped CuO powders used as target in the SPVD process and fig. 4b indicates the phases obtained after SPVD process.

In the case of pure and Mn doped CuO based powders, only the presence of the cooper (II) oxide crystalline phase can be observed on the XRD diffraction patters (the tenorite phase of CuO identified according to ICCD ASTM file no 01-089-5899. After SPVD process, it was observed that for small quantity of dopant (0.05 and 1%mol) all peaks in the XRD patterns can be indexed by the tenorite phase of CuO with a monoclinic structure; but in the case of 2.5 and 10%mol Mn doping a Mn3O4 tetragonal phase appear (identified by ICCD ASTM file no. 01-075-1560). That put in evidence the good doping for small percentage and an oxidation of Mn to Mn_3O_4 at large percentage in air pressure. Also, it was observed the presence of Cu_2O (ICDD ASTM file no. 04-016-6875) having a cubic crystallographic lattice. The diffraction peaks of the nanopowders are enlarged compared to those which are observed on CuO commercial pure powders. These XRD changes indicate important size effects.

The presence of Mn like dopant in the crystal structure of CuO is demonstrated by the slight movement to the left of the peaks. It was found nevertheless that the displacement increases when the Mn content increases like is shown in the Fig. 5 probably due to interstitial or substitution of Cu on the lattice. For this reason, the interplanar spacing increases, and, in accordance with the Bragg law, the diffraction peaks shift to the small angles.Rietveld analysis was performed with the help of WinPLOTR and FullProf software [17]. The microstructural effects are treated using the Voigt approximation: both instrumental and sample intrinsic profiles are supposed to be described approximately by a convolution of Lorentzian and Gaussian components. The TCH pseudo-Voigt profile function is used to mimic the exact Voigt function [17].

The integral breadth method to obtain volume averages of sizes and strains is used to output microstructural information which contains analysis of the size and strain contribution to each reflection. A phenomenological treatment of line broadening in terms of coherent domain size and strains due to structural defects (in our case Mn doping) can also be drawn also mentioned in other research [2].

During the SPVD process, the Mn atom substitute one of the Cu atoms or is interstitial placed in crystallographic lattice because in XRD patterns only a single phase appears. Because the radius of Mn atoms is largest then the radius of Cu atoms, this substitution conducts to a change in the lattice parameters, angle and strain like is shown in the Table 2.

This altering of structural parameters is due to the vapor condensation process and also to the doping effect of Mn.

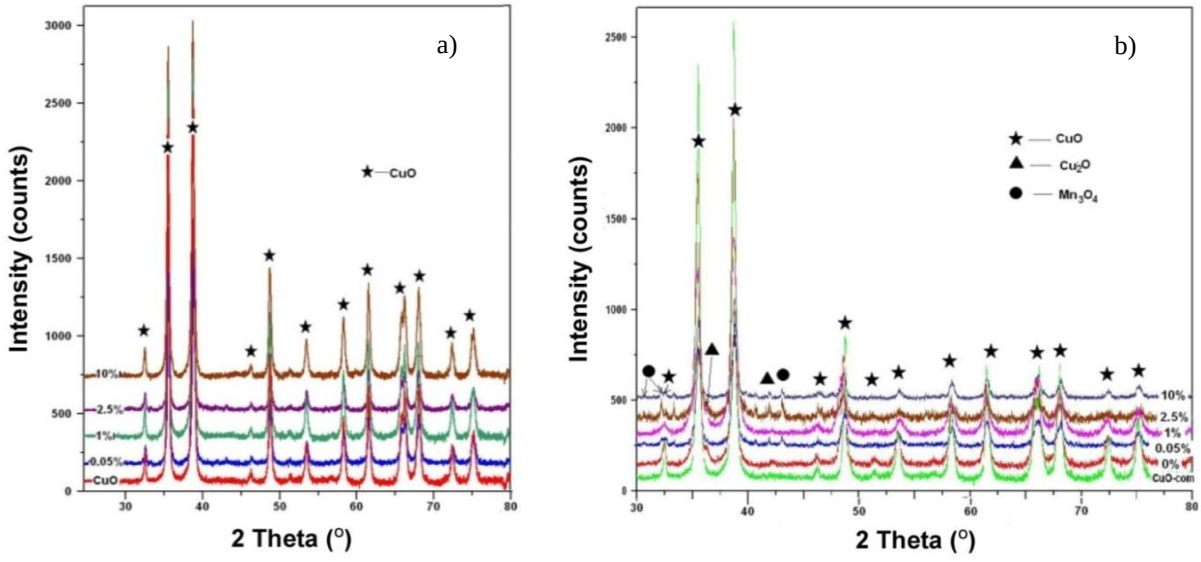

Fig. 4. X-ray patterns of a) commercial pure CuO and Mn-doped powders and b) pure and Mn-doped powders synthesised by S.P.V.D

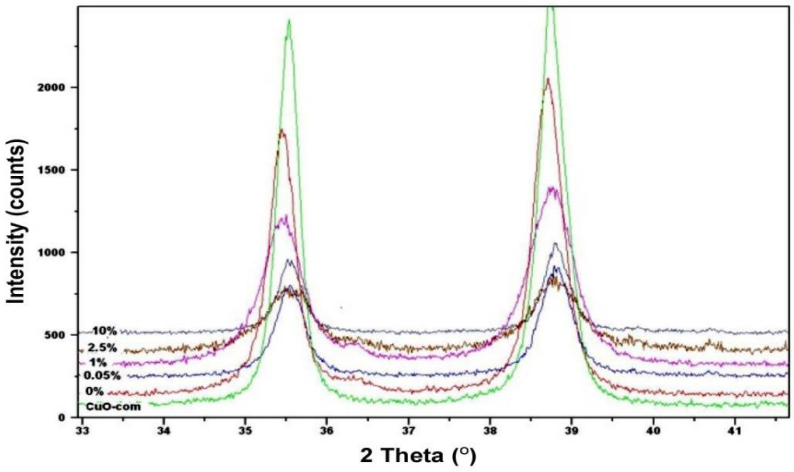

Fig. 5. The displacement and enlargement of peaks for CuO vapocondensed nanopowders

Tabel 2. Crystallographic parameters

Sample	**Lattice constants**			**β (°)**	**Average apparent size** (nm)	**Average maximum strain** (%%)	**Mean particle size obtained by TEM** (nm)
	a (Å)	b (Å)	c (Å)				
VCCuO	4.69041	3.42034	5.13205	99.6076	35.28	18.75	42
VC0.05MnCuO	4.69294	3.41986	5.13224	99.6354	24.48	33.56	36
VC1MnCuO	4.70828	3.40747	5.13113	99.8243	19.94	32.55	22
VC2.5MnCuO	4.70674	3.41402	5.13582	99.7128	22.30	56.28	32
VC10MnCuO	4.69923	3.41640	5.13046	99.7000	30.94	37.11	46

3.2. TEM analysis

In addition to XRD according to the TEM images of CuO nanostructures with different percent of Mn, it was found that the hexagonal CuO nanostructures were secondary form from self-assembly of many individual primary monoclinic nanoparticles. From literature [4] according to elaboration process was found that spherical structures self-assembled in cubic structure. The mechanism of the nanoparticles aggregating into cubic and hexagonal nanostructures indicated the flat pack process appears. The mean particle size obtained by TEM is comparable with the average apparent size from XRD presented in Table2.

The TEM image (Fig. 6) shows that the hexagonal or square consisted of CuO nanoparticles with the size between 22 and 46 nm. The analysis of TEM images demonstrates the influence of Mn like dopant, modifying the monoclinic structure of CuO probably due to the interstitial or substitution position in the crystal at small percentage of Mn and also the presence of cubic Cu_2O and Mn_3O_4 structures for 2.5 and 10%Mn doped nanopowdres.

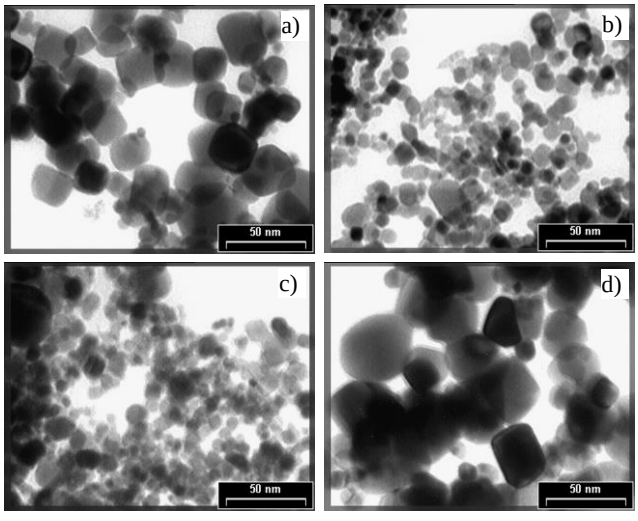

Fig. 6. TEM image of (a) pure CuO nanoparticles and doped with (b) 1% mol Mn (c) 2.5%mol Mn (d) 10%mol Mn

3.3 X-ray Fluorescence analysis

The XRF overlapped spectra of the SPVD synthesized CuO powders doped with 1, 2.5 and 10 %mol Mn are presented in Fig. 7.

EDXRF qualitative analysis clearly shows the presence of Mn within CuO nanopowders. Its concentration increases with the initial Mn adition from sample having 1%mol Mn, 2.5 %mol Mn up to 10%mol Mn.

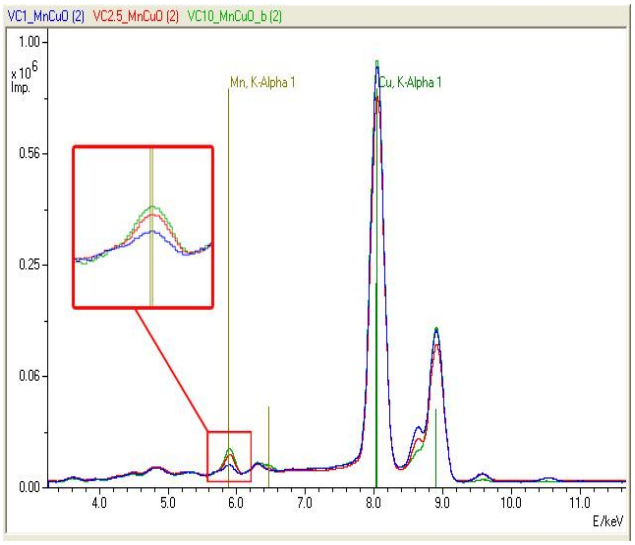

Fig. 7. EDXRF overlapped spectra of CuO nanopowders doped with a) 1%mol Mn b) 2.5%mol Mn and c) 10%mol Mn

The absence of any metallic Mn phase in XRD patterns for 1%mol Mn and in according with XRF qualitative analysis put in evidence that after the evaporation and condensation processes Mn might act like dopant in CuO structure.

4. Conclusions

To offer an alternative to chemical processes for oxide nanopowders, not totally satisfying; the challenge was to do that by SPVD as an original process to obtain nanopowders. The elaboration with solar energy of CuO nanoparticles pure and doped with Mn has not been reported yet. In the examples presented in the paper the nanostructured CuO powders were obtained from commercial targets. The diffraction peaks of the nanopowders are enlarged compared to those which are observed on CuO commercial pure powders wich indicate important size effects. The presence of Mn like dopant in the crystal structure of CuO is demonstrated by the slight movement to the left of the XRD peaks. In addition, according to the TEM images of CuO nanostructures with different percent of Mn, it was revealed that the hexagonal CuO nanostructures were secondary form from self-assembly of many individual primary monoclinic nanoparticles. EDXRF qualitative analysis clearly shows the presence of Mn within CuO nanopowders.

The present examples presented in the paper highlight the interest of elaboration CuO nanostructured powders using solar energy for future key applications.

Acknowlegements

All authors are indebted to SFERA Grant Agreement no. 228296), 7th EUprogram which has provided opportunities to work with the Odeillo solar facilities.

This work was supported by the strategic grant POSDRU/159/1.5/S/138963 - PERFORM, co-financed by the European Social Fund – Investing in People, within the Sectoral Operational Programme Human Resources Development 2007-2013.

References

[1] S. Asbrink, L.J. Norrby, Acta Crystalographica B, **26,** 8 (1970).
[2] X. Bokhimi, A. Morales, M.A. Lucatero, R. Ramírez, Nanostructured Materials, **9,** 315 (1997).
[3] V. Dhanasekaran, T. Mahalingam, R. Chandramohan, J. K. Rhee, J. P. Chu, Thin Solid Films **520,** 6608 (2012).
[4] W. Gao, S. Yang, S. Yang, L. Liya, Y. Du, Physics Letters A, **375,** 180 (2010).
[5] L. Guo, F. Tong, H. Liu, H. Yang, J. Li, Materials Letters, **71,** 32 (2012).
[6] J. Hongmei, M. Xiaowei, W. Lu, Q. Bin, Y. Gang, Powder Technology **241,** 43 (2013).
[7] Y. Jiang, J. Liao-Chuan, Z. Wei-De, G. Sundaram, Talanta, **82,** 25 (2010).
[8] T. Jan, J. Iqbal, M. Ismail, N. Badshah, Q. Mansoor, A. Arshad, Q. M. Ahkam, Materials Science in Semiconductor Processing, **21,** 154 (2014).
[9] J. Jayaprakasha, N. Srinivasanb, P. Chandrasekarana, E.K. Girijac, Spectrochimica Acta Part A: Molecular and Biomolecular Spectroscopy **136,** 1803**(C)**, (2015).
[10] J. Kouam, T. Ahcene-Ait, A.G. Plaiasu, M. Abrudeanu, A. Motoc, E. Beche, C. Monty, Solar Energy, **82,** 226 (2008).
[11] X. Liu, Z. Jiang, J. Li, Z. Zhang, L. Ren, Surface & Coatings Technology, **204**, 3200 (2010).
[12] R.N. Mariammal, K. Ramachandran, G. Kalaiselvan, S. Arumugam, B. Renganathanc, D. Sastikumar, Applied Surface Science, **270,** 545 (2013).
[13] C.J. A. Monty, The Arabian Journal for Science and Engineering, **35 (1C)**, 93 (2010).
[14] D. Negrea, C. Ducu, S. Moga, V. Malinovschi, C.J.A. Monty, B. Vasile, D. Dorobantu, M. Enachescu, Journal of Nanoscience and Nanotechnology, **12(11)**, 8746 (2012).
[15] A.G. Plaiasu, M. Abrudeanu, M.M. Dicu, C. Monty, J. Optoelectron. Adv. Mater. **16**(9-10), 1116 (2014).

[16] Z. Quan, E. Ni, Y. Ogasawara, N. Sonoyama, Solid State Ionics, **262,** 128 (2014).
[17] T. Roisnel, J. Rodriguez-Carvajal, "WinPLOTR: a Windows tool for powder diffraction patterns analysis", in R. Delhez and E.J. Mittenmeijer, eds. Materials Science Forum, Proceedings of the Seventh European Powder Diffraction Conference (EPDIC 7), Barcelona, 118, 2000.
[18] D.-M. Smilgies, Journal of Applied Crystallography, **42,** 1030 (2009).
[19] J. G. Zhao, S. J. Liu, S. H. Yang, S. G. Yang, Applied Surface Science, **257,** 9678 (2011).
[20] J. Yang, X. Kang, L. Hu, X. Gong, D. He, T. Peng, S. Mu, Journal of Alloys and Compounds, **572,** 158 (2013).
[21] Qiaobao Zhanga, Kaili Zhanga, Daguo Xua, Guangcheng Yangb, Hui Huangb, Fude Nieb, Chenmin Liuc, Shihe Yangd, Progress in Materials Science, **60,** 208 (2014).

*Corresponding author: plaiasugabriela@yahoo.fr